

Input Snapshots Fusion for Scalable Discrete Dynamic Graph Neural Networks

QingGuo Qi

qingguo21@mails.ucas.ac.cn

HangZhou Institute for Advanced Study
HangZhou, ZheJiang, China

Minhao Cheng

minhaocheng@ust.hk

Hong Kong University of Science and Technology
Hong Kong, China

Hongyang Chen*

dr.h.chen@ieee.org

Zhejiang Laboratory
Hangzhou, ZheJiang, China

Han Liu

liu.han.dut@gmail.com

Dalian University of Technology
Dalian, China

ABSTRACT

Dynamic graphs are ubiquitous in the real world, yet there is a lack of suitable theoretical frameworks to effectively extend existing static graph models into the temporal domain. Additionally, for link prediction tasks on discrete dynamic graphs, the requirement of substantial GPU memory to store embeddings of all nodes hinders the scalability of existing models. In this paper, we introduce an Input Snapshots Fusion based Dynamic Graph Neural Network (SFDyG). By eliminating the partitioning of snapshots within the input window, we obtain a multi-graph (more than one edge between two nodes). Subsequently, by introducing a graph denoising problem with the assumption of temporal decayed smoothing, we integrate Hawkes process theory into Graph Neural Networks to model the generated multi-graph. Furthermore, based on the multi-graph, we propose a scalable three-step mini-batch training method and demonstrate its equivalence to full-batch training counterpart. Our experiments, conducted on eight distinct dynamic graph datasets for future link prediction tasks, revealed that SFDyG generally surpasses related methods.

CCS CONCEPTS

- Theory of computation → Dynamic graph algorithms; • Information systems → Data mining.

KEYWORDS

Temporal Network, Scalable Graph Embedding, Learning Representation, Hawkes Process

ACM Reference Format:

QingGuo Qi, Hongyang Chen, Minhao Cheng, and Han Liu. 2018. Input Snapshots Fusion for Scalable Discrete Dynamic Graph Neural Networks. In *Proceedings of Make sure to enter the correct conference title from your*

*Corresponding author.

Permission to make digital or hard copies of all or part of this work for personal or classroom use is granted without fee provided that copies are not made or distributed for profit or commercial advantage and that copies bear this notice and the full citation on the first page. Copyrights for components of this work owned by others than the author(s) must be honored. Abstracting with credit is permitted. To copy otherwise, or republish, to post on servers or to redistribute to lists, requires prior specific permission and/or a fee. Request permissions from permissions@acm.org.

Conference acronym 'XX, June 03–05, 2018, Woodstock, NY

© 2018 Copyright held by the owner/author(s). Publication rights licensed to ACM.

ACM ISBN 978-1-4503-XXXX-X/18/06

<https://doi.org/XXXXXX.XXXXXXX>

rights confirmation email (Conference acronym 'XX). ACM, New York, NY, USA, 13 pages. <https://doi.org/XXXXXX.XXXXXXX>

1 INTRODUCTION

Graphs are prevalent in the real world, appearing diverse domains such as social networks [5, 33], molecule graphs [24], and traffic networks [19, 36]. They serve as powerful representations capturing relationships or interactions between entities. Traditional graph representation learning has predominantly focused on static graphs characterized by fixed nodes and edges [9, 31]. However, real-world graphs often undergo dynamic changes, with the graph structure evolving over time [23]. The pursuit of learning dynamic graph representations has thus become a pivotal research challenge. Existing methods for dynamic graph representation learning fall into two broad categories [14]: continuous-time methods and discrete-time methods. Continuous-time methods conceptualize the evolution of dynamic graphs as an event stream, modeling continuous temporal information through mechanisms like point processes or time random walks [4, 17, 27, 29, 32]. However, acquiring the most recent data promptly to update models in practical applications can pose a challenge, leading to potential discrepancies between training data and application scenarios. On the other hand, discrete-time methods treat dynamic graphs as sequences of snapshots at discrete time points. These approaches employ techniques like Graph Neural Networks (GNNs) [9, 31] to capture graph features. Additionally, they integrate time encoders, such as Recurrent Neural Networks (RNNs) [3, 11] or Transformers [30], to encode the dynamics of each node over time [23, 28, 34, 35, 37, 38]. This discrete-time paradigm provides a practical approach to model dynamic graph evolution, enabling effective representation learning that aligns with real-world applications.

While discrete dynamic graph representation learning has demonstrated success, its scalability is constrained by the necessity for full-batch training on the input graph. Several strategies have been proposed in the literature to overcome this limitation, such as utilizing latent random variables [8], utilizing hyperbolic space [34], and leveraging meta-learning methods [35]. These approaches enable the system to process a single snapshot as input, offering a promising solution for scalability. By sequentially training multiple snapshots, existing static graph scaling techniques can be utilized. However, it should be noted that the training time scales linearly

with the total number of snapshots. Moreover, disregarding long-distance time dependencies may lead to overfitting issues, arising from the potential biases introduced by local optima in the training process.

To address the aforementioned challenges and strike a balance between long-range dependencies and scalability, we introduce a novel approach called "input snapshots fusion." This method involves consolidating multiple input snapshots into a multi-graph structure, allowing for the existence of multiple edges between two nodes. This innovative technique opens up a new domain in graph representation learning, specifically focusing on multi-graphs with temporal attributes assigned to edges. Specifically, we leverage the theory of Hawkes processes to model temporal edges between node pairs, formulating it as a graph denoising problem with a time decay smoothing assumption. This formulation leads to the development of a time decay message passing mechanism, showcasing the integration of Hawkes processes with Graph Convolutional Networks (GCN) [16] and Graph Attention Networks (GAT) [31]. Various adaptations can be generated by utilizing distinct Laplacian operators. Moreover, for the link prediction task in discrete dynamic graphs, storing all node embeddings on the GPU for contrastive learning is a common practice that often poses a scalability bottleneck. To overcome this challenge, we propose a scalable mini-batch training algorithm consisting of three steps, ensuring equivalence to the full-batch version. This approach enables the application of the model on large-scale datasets.

Extensive experiments conducted on eight widely used public datasets demonstrate that our approach outperforms state-of-the-art baselines significantly in link prediction tasks. The adoption of our proposed mini-batch training approach substantially reduces the demand for GPU memory, achieving a maximum reduction of 50%. Furthermore, ablation studies confirm the effectiveness of the proposed Hawkes process-based Graph Neural Network in accurately modeling multi-graphs, resulting in a potential enhancement of up to 2.5 times compared to conventional graph neural networks.

In summary, the main contributions are as follows:

- We introduce the novel concept of input snapshots fusion, addressing the challenge of learning representations for temporal attribute multi-graphs in discrete dynamic graphs. This method consolidates multiple input snapshots into a multi-graph structure, paving the way for a more comprehensive understanding of the temporal evolution of graph data.
- Leveraging Hawkes processes theory, we formulate a graph denoising problem with a time decay smoothing assumption. This innovative approach allows us to model temporal edges between node pairs, leading to the development of Graph Neural Networks (GNNs) with a time decay message passing mechanism.
- Recognizing the challenges posed by storing all node embeddings on the GPU for contrastive learning in link prediction tasks, we propose a scalable mini-batch training algorithm. This algorithm ensures equivalence to the full-batch version, addressing scalability issues and facilitating the application of our model on large-scale datasets.
- We conduct extensive experiments to validate the effectiveness of our proposed model. The experiments demonstrate

the superior performance of our approach in link prediction tasks on eight widely used public datasets.

2 PRELIMINARIES

In this section, we introduce notations for discrete dynamic graph and briefly summarize several important models.

A discrete dynamic graph is defined as a series of snapshots $\{\mathcal{G}^1, \mathcal{G}^2, \dots, \mathcal{G}^T\}$, where T is the total number of snapshots. The snapshot at time t , i.e., $\mathcal{G}^t = (\mathcal{V}^t, \mathcal{E}^t)$ is a graph with a node set \mathcal{V}^t and an edge set $\mathcal{E}^t \subseteq \mathcal{V}^t \times \mathcal{V}^t$, where \mathcal{E}_{ij}^t represents an edge from node i to node j at snapshot t . We use \mathbf{A}^t to denote the binary adjacency matrix corresponding to the edge set \mathcal{E}^t . The superscript "t" can be omitted when it is not specified. In our study, we use symbol $\tilde{\cdot}$ to denote notions related to multi-graph where multiple edges at different timestamps may exist between two nodes. In this case, an edge set $\tilde{\mathcal{E}} \subseteq \mathcal{V} \times \mathcal{V} \times T'$, where T' are available timestamps of all edges and $\tilde{\mathcal{E}}_{ijt'}$ represents an edge from node i to node j at timestamp t' . The neighbors of node i , denoted as \tilde{N}_i is a set of edges with target node id and timestamp, $\{(j, t') | (i, j, t') \in \tilde{\mathcal{E}}\}$ where j represents the index of the neighboring node, while t' denotes the timestamp of the edge. It is important to clarify that in our notation, t is assigned for snapshot indexing, whereas t' is specifically used for edge timestamp.

In the following, we generally use $\mathbf{H}^l \in \mathbb{R}^{n \times d}$ to denote the l -th layer output of GNN where $n = |\mathcal{V}|$ is the number of nodes and d is the dimension of embedding, and \mathbf{H}_i is used to denote corresponding i -th row. Next, we describe a few important models.

2.1 Link Prediction in Discrete Dynamic Graphs

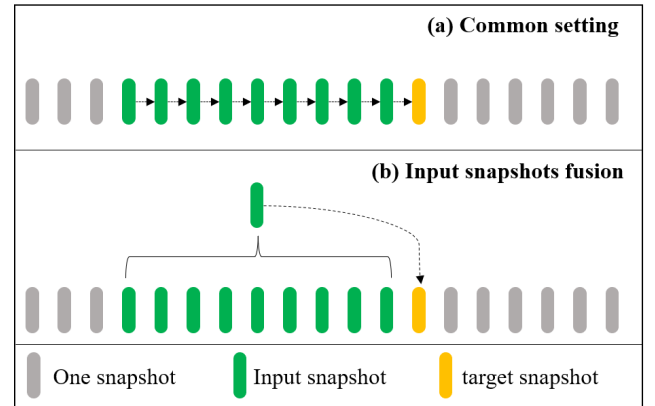


Figure 1: Training setting for the task of link prediction in dynamic graphs.

In dynamic graphs, a sliding time window of length w is commonly employed, where $w \geq 2$ is a configurable hyperparameter. For the link prediction task, the final snapshot within the sliding window is designated as the target, while the preceding $w - 1$ snapshots serve as input data for predicting edges in the target snapshot. These snapshots are categorized into training, validation, and test sets according to the location of the target snapshot. Figure 1(a) depicts a typical training scenario utilizing multiple snapshots as

input, while Figure 1(b) presents the input snapshot fusion method, to be elaborated upon later in section 3.1.

2.2 Graph Convolutional Networks

A single GCN layer [16] can be written as follows:

$$\mathbf{H}^{l+1} = \hat{\mathbf{A}} \mathbf{H}^l \mathbf{W},$$

where $\mathbf{W} \in \mathbb{R}^{d \times d}$ is a feature transformation matrix, and $\hat{\mathbf{A}}$ is a normalized adjacency matrix. Additionally, from the perspective of message passing [7], the update formula for node i can be defined as

$$\mathbf{H}_i^{(l+1)} = \sum_{j \in \mathcal{N}(i) \cup \{i\}} \frac{1}{\sqrt{\deg(i)} \cdot \sqrt{\deg(j)}} \cdot \left(\mathbf{W}^\top \mathbf{H}_j^{(l)} \right), \quad (1)$$

where neighboring node features are first transformed by the weight matrix \mathbf{W} , normalized by their degree, and finally summed up.

2.3 Graph Attention Networks

Graph Attention Networks (GAT) [31] adopts the same message passing mechanism as GCN. The feature aggregation operation for node i is defined as:

$$\mathbf{H}_i^{l+1} = \sum_{j \in \mathcal{N}(i)} \alpha_{ij} \mathbf{H}_j^l, \quad \text{with} \quad \alpha_{ij} = \frac{\exp(e_{ij})}{\sum_{k \in \mathcal{N}(i)} \exp(e_{ik})}. \quad (2)$$

where $\mathcal{N}(i) = \mathcal{N}(i) \cup \{i\}$ denotes i 's neighbors (self-inclusive), and \mathbf{H}_i is the i -th row of \mathbf{H} , i.e. the output features of node i . In this aggregation operation, α_{ij} is a learnable attention score to differentiate the importance of distinct nodes in the neighborhood. Specifically, α_{ij} is a normalized form of e_{ij} , which is modeled as:

$$e_{ij} = \text{LeakyReLU} \left(\left[\mathbf{X}'_i \| \mathbf{X}'_j \right] \mathbf{a} \right), \quad (3)$$

where $[\cdot \| \cdot]$ denotes the concatenation operation and $\mathbf{a} \in \mathbb{R}^{2d}$ is a learnable vector.

2.4 GNNs as Solving Graph Denoising Problem

According to the conclusion in [21], GNN models can be regarded as an approximation for solving a graph denoising problem under the assumption of smoothness. Formally, Given a noisy input signal $\mathbf{S} \in \mathbb{R}^{N \times d}$ on a graph \mathcal{G} , the goal is to recover a clean signal $\mathbf{F} \in \mathbb{R}^{N \times d}$, assumed to be smooth over \mathcal{G} , by solving the following optimization problem:

$$\arg \min_{\mathbf{F}} \mathcal{L} = \|\mathbf{F} - \mathbf{S}\|_F^2 + \lambda \cdot \text{tr}(\mathbf{F}^\top \mathbf{L} \mathbf{F}). \quad (4)$$

Where the first term guides \mathbf{F} to be close to \mathbf{S} , while the second term $\text{tr}(\mathbf{F}^\top \mathbf{L} \mathbf{F})$ is the Laplacian regularization which guides \mathbf{F} 's smoothness over \mathcal{G} , with $\lambda > 0$'s mediation.

2.5 Hawkes Process

The Hawkes process is a typical temporal point process [39] that describes a sequence of discrete events by assuming that previous events have an impact on the current, with the influence diminishing over time. A univariate Hawkes process is defined to be a

self-exciting temporal point process N whose conditional intensity function $\lambda(t)$ is defined to be

$$\lambda(t) = \mu(t) + \sum_{i: \tau_i < t} \kappa(t - \tau_i), \quad (5)$$

where $\mu(t)$ is background rate of the process N , τ_i are the points in time occurring prior to time t ; κ is a exciting function that models the time decay effect of past history on the current event, which is usually in the form of an exponential function,

$$\kappa(t - s) = \exp(-\delta(t - s)), \quad (6)$$

where the δ is a non-negative source dependent parameter, representing the time sensitivity of the process N .

3 THE SFDYG MODEL

In this section, we introduce the proposed SFDyG framework. First, we discuss the feasibility and advantages of input snapshot fusion. Then, we propose a graph neural network based on Hawkes processes to address the case of multiple edges between two vertices. It has been proved that our model extends the graph denoising problem to temporal domain which considers the effect of time decay. Furthermore, we present a mini-batch training method for the task of discrete dynamic graph link prediction, which makes our model scalable to large datasets. Finally, we analyze the complexity of SFDyG and compare it with existing methods, demonstrating that SFDyG framework is scalable and fast after the adoption of input snapshot fusion.

3.1 Input Snapshots Fusion

We found that direct utilization of the coarsely partitioned snapshots as input for the model is deemed sub-optimal. The time information at the edges is discretized into snapshot numbers, leading to a loss of valuable information. Drawing from this insights, as shown in Figure 1(b), we propose a method called input snapshots fusion, denoted as SF , which amalgamates edges from input snapshots of sliding window into a single graph structure with multiple edges between two vertices, namely a multi-graph. Formally,

$$\tilde{\mathcal{G}} = SF(\mathcal{G}^1, \dots, \mathcal{G}^{w-1}) = (\mathcal{V}, \mathcal{E}^1 \cup \dots \cup \mathcal{E}^{w-1}), \quad (7)$$

where $\mathcal{G}^1, \dots, \mathcal{G}^{w-1}$ are the input snapshots in the sliding window and \cup represents union of two edge sets.

The essence of input snapshots fusion is not to artificially partition the input snapshots. As depicted in Figure 2, this process yields a multi-graph characterized by multiple edges connecting two nodes, with each edge possessing timestamp information indicating its occurrence time. The presence of multiple edges indicates a multitude of events that have occurred among the nodes over time, motivating us to model them using Hawkes processes.

3.2 Hawkes Process Based GNN

According to the theory of Hawkes processes, the connections that have occurred between two nodes have an excitatory effect on their subsequent occurrences. Hence, an Hawkes excitation matrix C can be defined,

Definition 3.1 (Hawkes excitation matrix). Assuming below that the edges are undirected, a symmetric matrix C where each element

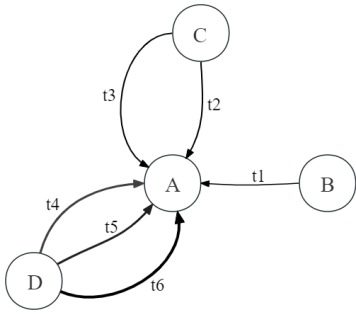


Figure 2: An example of the generated multi-graph resulting from the fusion of input snapshots. The thickness of each edge is indicative of the time proximity.

C_{ij} represents the influence of all previously occurred edges from node i to node j on the future,

$$C_{ij} = \sum_{(i,j,t') \in \tilde{E}_i} \exp(-\delta_i(\tau - t')), \text{ with } t' < \tau. \quad (8)$$

Where t' denotes the timestamp of an edge, while τ denotes the timestamp to be predicted. Additionally, the non-negative scalar parameter δ_i describes the time sensitivity of the source node i . Then, the subsequent definitions can be derived.

Definition 3.2 (Hawkes adjacency matrix). The dot product of Hawkes excitation matrix C and the graph adjacency matrix A

$$\tilde{A} = C \cdot A. \quad (9)$$

Where A is a binary symmetric matrix, where 1 represents the existence of at least one edge between two nodes.

Definition 3.3 (Degree matrix of Hawkes adjacency matrix). A diagonal matrix created by summing the elements in each row of the Hawkes adjacency matrix.

$$\tilde{D} = \text{diag}(\sum_j \tilde{A}_{ij}). \quad (10)$$

Based on these definitions, the relationship between Hawkes processes and graph denoising can be established in Theorem 3.1.

THEOREM 3.1 (HAWKES GRAPH DENOISING). *When we adopt the hawkes Laplacian matrix $\tilde{L} = \tilde{D} - \tilde{A}$, the graph denoising problem (Equation 4) was extended to temporal domain with the assumption that the smoothness of edges decays over time.*

PROOF.

$$\begin{aligned} \lambda \cdot \text{tr}(\mathbf{F}^\top \tilde{L} \mathbf{F}) &= \lambda \cdot \sum_{(i,j) \in \mathcal{E}} C_{ij} \|\mathbf{F}_i - \mathbf{F}_j\|_2^2 \\ &= \lambda \cdot \sum_{(i,j) \in \mathcal{E}} \sum_{(i,j,t') \in \tilde{E}_i} \exp(-\delta_i(\tau - t')) \|\mathbf{F}_i - \mathbf{F}_j\|_2^2 \\ &= \lambda \cdot \sum_{(i,j,t') \in \tilde{E}} \exp(-\delta_i(\tau - t')) \|\mathbf{F}_i - \mathbf{F}_j\|_2^2. \end{aligned} \quad (11)$$

Where each element of the summation is in the form of a time decay coefficient multiplied by a graph smoothing indicator. which completes the proof. \square

Clearly, as one edge ages, the smooth constraint between the two endpoints decreases continuously, which is consistent with our intuition. Furthermore, by applying the results from the paper [21], the graph denoising problem can be (approximately) regraded as GNN models. As a result, it is possible to derive Hawkes process based GNNs.

3.2.1 Hawkes+GCN. By adopting the normalized Hawkes Laplacian matrix $\tilde{L} = \tilde{D}^{-\frac{1}{2}} (\tilde{D} - \tilde{A}) \tilde{D}^{-\frac{1}{2}}$ in Equation 4, the graph denoising problem is connected to the GCN model [21]. Formally,

$$\mathbf{H}^{k+1} = \tilde{D}^{-\frac{1}{2}} \tilde{A} \tilde{D}^{-\frac{1}{2}} \mathbf{H}^k \mathbf{W}, \quad (12)$$

where $\mathbf{H}^0 = \mathbf{X}$ and the i -th element in the node embedding \mathbf{H} can be represented in the following form,

$$\begin{aligned} \mathbf{H}_i^{(k+1)} &= \sum_{j \in N(i)} \frac{C_{ij}}{\sqrt{\deg(i)\deg(j)}} \cdot \mathbf{W}^\top \mathbf{H}_j^{(k)} \\ &= \sum_{(j,t') \in \tilde{N}(i)} \frac{\exp(-\delta_i(\tau - t'))}{\sqrt{\deg(i)\deg(j)}} \mathbf{W}^\top \mathbf{H}_j^{(k)}. \end{aligned} \quad (13)$$

Where $\deg(i)$ represents the degree of node i of the binary adjacency matrix A and δ_i is an adaptive parameter that describes the temporal sensitivity of a node. Based on the formula, we derived a time-decayed message passing mechanism on multi-graph. It is important to note that the Laplacian matrix \tilde{L} may have eigenvalues greater than 1 as a consequence of multiple edges between two nodes. Therefore, we suggest incorporating batch normalization [13] into the model to mitigate the issue of numerical instability.

3.2.2 Hawkes+GAT. The success of GAT is to calculate the non-negative attention score α_{ij} to differentiate the importance of distinct nodes in the neighborhood, which is a natural choice of the time sensitivity coefficient δ in Equation 13. Then, the GAT model is extended to temporal domain, Formally,

$$\begin{aligned} \mathbf{H}_i^{(k+1)} &= \sum_{(j,t') \in \tilde{N}(i)} \frac{\exp(-\delta_{ij}(\tau - t'))}{\sqrt{\deg(i)\deg(j)}} \mathbf{H}_j^{(k)} \mathbf{W}^T, \\ \text{with } \delta_{ij} &= \frac{\exp(e_{ij})}{\sum_{k \in N(i)} \exp(e_{ik})}. \end{aligned} \quad (14)$$

Where e_{ij} is described in Equation 3. In this way, the hawkes based GAT is derived under the assumption that the time sensitivity dependents on both the source and target node of an edge, enabling more flexible modeling.

3.3 Scalable minibatch Training algorithm

In this subsection, we propose a scalable mini-batch training algorithm specifically for link prediction tasks. We demonstrate that by adopting the **input snapshot fusion** method, we can easily employ existing training algorithms to enable the application of our model to large-scale dynamic graph datasets.

For our GNN based dynamic graph models for link prediction, there are mainly two components: an GNN based encoder, referred to as \mathcal{G} , which generates node embeddings \mathcal{H} for all vertices based

on the input graph, and a decoder called \mathcal{F} , which is a multi-layer perceptron (MLP) responsible for predicting the probability of future connections between two nodes based on their embeddings. The forward propagation process can be formalized as:

$$\mathcal{H} = \mathcal{G}(\text{data}), z_{ij} = \mathcal{F}(\mathcal{H}_i, \mathcal{H}_j), \hat{y}_{ij} = \sigma(z_{ij}), \quad (15)$$

where the term data refers to the whole multi-graph structure generated by the process of input snapshot fusion. \mathcal{H}_i represents the embedding of node i , and \hat{y}_{ij} denotes the likelihood of a future connection from node i to node j which is obtained by employing sigmoid on the intermediate result z_{ij} . Consistent with existing research, for each edge in the training set, k random negative edges are sampled, and the cross-entropy loss is used as the loss function:

$$\mathcal{L} = \frac{1}{|\tilde{E}|} \sum_{e_{ij} \in \tilde{E}} (-y_{ij} \cdot \log(\hat{y}_{ij}) \cdot k - (1 - y_{ij}) \cdot \log(1 - \hat{y}_{ij})). \quad (16)$$

Where $\tilde{E} = \mathcal{E}_{\text{pos}} \cup \mathcal{E}_{\text{neg}}$ is the union of all positive edges and negative sample edges of the target snapshot and the y_{ij} represents the ground truth edge label of the edge e_{ij} . The loss term of the positive samples is multiplied by k to balance the number of positive and negative samples.

Obviously, both the \mathcal{G} and the \mathcal{F} can be transformed into mini-batch using existing methods [1, 2, 9, 18, 22, 25, 26], while the intermediate result \mathcal{H} is a bottleneck of scalability. Assuming that \mathcal{H} can be accommodated in the memory but not the GPU memory, since the memory of a computer is usually much larger. Then, the problem is transformed into how to move \mathcal{H} outside of GPU while achieving gradient backward propagation.

The backward propagation of gradients can be divided into two stages. In the first stage, $\frac{\partial \mathcal{L}}{\partial \mathcal{F}}$ is used to update the parameters of \mathcal{F} , and in the second stage, $\frac{\partial \mathcal{L}}{\partial \mathcal{H}} \frac{\partial \mathcal{H}}{\partial \mathcal{G}}$ is used to update the parameters of \mathcal{G} . Therefore, a three-step mini-batch training method was derived:

- (1) using mini-batch graph training to get \mathcal{H} , save values in memory,
- (2) train \mathcal{F} using \mathcal{H} via mini-batch training and collect $\mathcal{H}_{\text{grad}}$, the gradient of \mathcal{H} ,
- (3) using mini-batch graph training to update parameters of \mathcal{G} via $\mathcal{H}_{\text{grad}}$

A detailed description of the scalable training algorithm can be found in Algorithm 1. Where the `batch.node_id` represents seed nodes selected in each mini-batch and the partial gradients are provided by the auto gradient function of training framework, i.e pytorch. While the accumulate gradient keyword means the gradient for each mini-batch is summed up and the model parameters are updated outside the for loop. Furthermore, we have provided additional validation analysis to prove that the mini-batching training has the same effect as the original full-batch training algorithm when the sampled negative edges are same (see Appendix A.2).

3.4 Complexity Analysis

In this subsection, time and space complexity analyses were provided for SFDyG and the following representative DGNNs: DySAT [28], EvolveGCN [23] and ROLAND [35].

In the context of discrete dynamic graph link prediction, we consider several parameters to analysis the complexity of Encoder

Algorithm 1: Mini-batch Training for SFDyG

```

Input: Encoder  $\mathcal{G}$ , decoder  $\mathcal{F}$ , mini-batch graph loader
Loader, all training edges  $\tilde{E}$ 
Output: Updated  $\mathcal{G}$ ,  $\mathcal{F}$ 
1 Initialize  $\mathcal{H} \leftarrow 0$ ,  $\mathcal{H}_{\text{grad}} \leftarrow 0$ ;
2 while not converge do
3   for batch in Loader do
4     id  $\leftarrow$  batch.node_id ;
5      $\mathcal{H}[\text{id}] \leftarrow \mathcal{G}(\text{batch}).\text{detach}().\text{cpu}()$  ;
6   end
7   for batch in  $\mathcal{E}$  do
8      $h1 \leftarrow \mathcal{H}[\text{batch}.src].\text{cuda}()$  ;
9      $h2 \leftarrow \mathcal{H}[\text{batch}.dst].\text{cuda}()$  ;
10    label  $\leftarrow$  batch.edge_label ;
11     $\mathcal{L} \leftarrow \frac{1}{|\tilde{E}|} \text{cross\_entropy}(\mathcal{F}(h1, h2), \text{label}).\text{sum}()$  ;
12    accumulate  $\frac{\partial \mathcal{L}}{\partial \mathcal{F}}$  ;
13     $\mathcal{H}_{\text{grad}}[\text{batch}.src] += \frac{\partial \mathcal{L}}{\partial h1}.\text{cpu}()$  ;
14     $\mathcal{H}_{\text{grad}}[\text{batch}.dst] += \frac{\partial \mathcal{L}}{\partial h2}.\text{cpu}()$  ;
15  end
16  update  $\mathcal{F}$  using accumulated  $\frac{\partial \mathcal{L}}{\partial \mathcal{F}}$  ;
17  for batch in Loader do
18    id  $\leftarrow$  batch.node_id ;
19     $h \leftarrow \mathcal{G}(\text{batch})$  ;
20    accumulate  $\frac{\partial \mathcal{L}}{\partial \mathcal{G}} \leftarrow \frac{\partial h}{\partial \mathcal{G}} \cdot \mathcal{H}_{\text{grad}}[\text{id}].\text{cuda}()$  ;
21  end
22  update  $\mathcal{G}$  using accumulated  $\frac{\partial \mathcal{L}}{\partial \mathcal{G}}$  ;
23 end

```

Table 1: Comparison of time and memory complexities.

Method	Time	Memory
DySAT	$O(TL E F + TL N F^2)$	$O(TL N F + TLF^2)$
EvolveGCN	$O(TL E F + TL N F^2)$	$O(TL N F + TLF^2)$
Roland	$O(L E F + L N F^2)$	$O(L E F + LF^2)$
SFDyG-F	$O(TL E F + L N F^2)$	$O(TL E F + LF^2)$
SFDyG-B	$O(Nd^L F^2)$	$O(bd^L F + LF^2)$

\mathcal{G} in one time window. The total number of snapshots is denoted as S , the training unit is a time window with a length of T , and the total number of nodes is represented as $|N|$. Moreover, we have the average number of edges per snapshot denoted as $|E|$, and the average degree per node as d . Without loss of generality, we assume that the node feature dimension and the length of the hidden vectors in the network are both F . Additionally, the number of layers in the graph neural network is represented as L , and the batch size for mini-batch training is denoted as b . The time and memory complexities are summarized in Table 1, while detailed analysis are provided in Appendix A.3.

Overall, the full-batch version denoted as SFDyG-F exhibits the second-best time and space complexity, only surpassed by roland. In comparison to roland, SFDyG demonstrates enhanced capability in capturing long-range temporal dependencies, without being constrained by sequential training (in time order). while the mini-batch

version denoted as SFDyG-B showcases superior space complexity, making it suitable for application in large-scale dynamic graphs with numerous nodes.

4 EXPERIMENTS

4.1 Experimental Setup

4.1.1 Datasets. We conducted experiments on eight commonly used public datasets that have been extensively evaluated in previous studies on dynamic graph representation learning, encompassing Bitcoin-Alpha, Bitcoin-OTC, UCI, Reddit-Title, Body, AS733 and Stack Overflow. The fundamental statistics of the eight datasets are presented in Table 3. Following EvolveGCN [23], we subdivided the original dataset into multiple snapshots of equal frequency. Subsequently, the training, validation, and test sets are divided along the time dimension. Details of the datasets can be found in Appendix B.1.

4.1.2 Baselines. We assess the performance of our proposed model, SFDyG-GCN, SFDyG-GAT, by comparing it to several dynamic GNN baselines, namely EvolveGCN [23], DySAT [28], ROLAND [35], VGRNN [8], HTGN [34] and WinGNN [38]. In Appendix B.2, a comprehensive description of these baselines can be found.

4.1.3 Evaluation metrics. We evaluate the effectiveness of SFDyG framework in the context of future link prediction. Our primary evaluation metric is the Mean Reciprocal Rank (MRR) with 100 negative sampling as defined in OGB [12], which is an average of the pessimistic and optimistic ranks. An analysis of different MRRs based on various statistical approaches are presented in Appendix B.3. Additionally, performance metrics such as hits@1, hits@3, hits@10 are also provided in Appendix B.5.

4.1.4 SFDyG Architecture. SFDyG adopts the prevalent encoder-decoder architecture for future link prediction, featuring a two-layer hawkes process based GNN as the encoder to generate embeddings for all nodes. The model utilizes a two-layer MLP as the decoder, taking a pair of nodes as input and determining the probability of their forthcoming connection. To maintain parity in evaluations, all models in the experiment share identical decoders architecture, differing only in their encoders.

4.2 Main Results

4.2.1 Full-batch Training. The performance of the proposed SFDyG and other baseline models in dynamic link prediction is presented in Table 2. The results reveal significant variations in the effectiveness of existing baseline models across different dynamic graph datasets. DySAT and EvolveGCN, equipped with temporal encoders, demonstrate better performance on denser datasets like AS733 and SBM, suggesting possible under-utilization of temporal encoders. Conversely, models with single snapshot inputs, such as VGRNN and HTGN, exhibit similar performances, indicating potential neglect of temporal features. Roland emerges as the top performer among all baseline models, likely attributable to its meta-learning approach that utilizes historical data from the test set in training. In contrast, our proposed model SFDyG showcases substantial advantages over all datasets, outperforming baseline models by a considerable margin, highlighting the efficacy of our GNN based on Hawkes

processes in capturing temporal information in multi-graphs. Generally, SFDyG-GAT demonstrates slightly superior performance compared to SFDyG-GCN, except for datasets with minimal edges like bitcoin-alpha and nodes like SBM, thereby affirming the more adaptable modeling capability of SFDyG-GAT. Collectively considering these factors, we assert that SFDyG surpasses existing baseline methods in dynamic link prediction capabilities.

Figure 3 illustrates the utilization of GPU memory by the SFDyG model throughout the training procedure as compared to various standard baseline methods. The findings demonstrate a notable superiority of our approach over other multi-snapshot input baselines, some of which face out-of-memory (OOM) issues when applied to the StackOverflow dataset. Our GPU memory consumption closely resembles that of the single snapshot input method Roland, exhibiting a lower constant space complexity, albeit performing less effectively than Roland when applied to the SBM dataset with an edge density about 100. The higher efficiency in memory usage of our method suggests promising scalability potential.

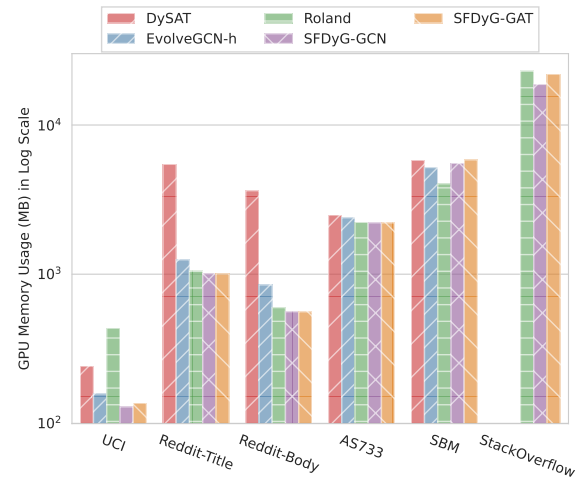


Figure 3: The GPU memory usage of SFDyG and representative baselines on six datasets.

4.2.2 Mini-batch Training. While it is theoretically possible to demonstrate the equivalence of the proposed mini-batch training method to the full-batch training version, practical implementation faces challenges in ensuring identical negative sampling samples between the two methods. To address this issue, oversampling trick was employed in our experiments. During mini-batch data generation, we sampled 4-hop neighbors for each seed node for our two-layer GNN model to increase the pool of nodes available for negative sampling. Specifically, a uniform random neighbor sampling approach was adopted, with sampling sizes of 20, 10, 5, and 1 for each hop. The batch size remained constant at 1024.

The comparative results of full-batch training and mini-batch training are presented in Table 4. The findings suggest that employing mini-batch training techniques on SFDyG-GCN and SFDyG-GAT yield similar outcomes. Generally, due to the introduction of randomness in random neighbor sampling, the results of full-batch training and mini-batch training are not identical, but the variance

Table 2: Overall performance (MRR@100) comparison on eight datasets (% is omitted). Our experiments guarantee consistent data settings, and standardized methods for computing Mean Reciprocal Ranks (MRRs) to facilitate fair comparisons. Each experiment is conducted using three random seeds, and the average performance is reported along with the standard error.

Methods	OTC	Alpha	UCI	Title	Body	AS733	SBM	SO
DySAT	3.00 ± 0.68	3.33 ± 1.79	3.72 ± 1.59	2.86 ± 0.47	2.85 ± 1.06	19.92 ± 0.74	4.28 ± 1.57	OOM.
Evolve-o	7.90 ± 0.15	6.66 ± 0.44	7.22 ± 0.05	OOM.	18.45 ± 0.02	42.06 ± 0.00	21.38 ± 0.00	OOM.
Evolve-h	7.08 ± 0.10	6.82 ± 0.37	6.04 ± 1.70	30.64 ± 0.02	18.46 ± 0.02	42.06 ± 0.00	21.38 ± 0.00	OOM.
VGRNN	6.60 ± 0.33	6.84 ± 0.28	7.05 ± 0.15	OOM.	OOM.	42.38 ± 0.79	19.70 ± 0.53	OOM.
Roland	28.25 ± 0.51	29.41 ± 0.68	19.85 ± 2.40	46.77 ± 0.37	39.29 ± 0.40	39.80 ± 5.24	2.70 ± 1.05	37.16 ± 0.07
WinGNN	4.07 ± 0.85	3.73 ± 0.87	3.10 ± 0.81	6.26 ± 0.76	3.55 ± 1.17	6.93 ± 1.59	3.21 ± 0.17	OOM.
HTGN	5.99 ± 1.20	5.75 ± 0.56	8.06 ± 2.90	25.06 ± 1.83	15.26 ± 7.26	11.79 ± 4.51	OOM.	OOM.
SFDyG-GCN	34.47 ± 0.13	31.77 ± 0.42	30.19 ± 0.22	42.67 ± 0.58	27.95 ± 0.66	45.76 ± 0.14	24.23 ± 0.21	44.25 ± 0.10
SFDyG-GAT	37.37 ± 0.10	30.33 ± 1.05	32.58 ± 1.02	50.44 ± 0.16	40.46 ± 0.53	46.53 ± 0.49	24.02 ± 4.55	46.13 ± 0.05

Table 3: The statistics of eight datasets used in the experiment.

	# Nodes	# Edges	# Time Steps (Train / Val / Test)	Avg. Degree
UCI	1,899	59,835	35 / 5 / 10	0.36
Alpha	3,777	24,173	95 / 13 / 28	0.04
OTC	5,881	35,588	95 / 14 / 28	0.05
Title	54,075	571,927	122 / 35 / 17	0.06
Body	35,776	286,562	122 / 35 / 17	0.05
AS733	7,716	1,167,892	70 / 10 / 20	2.12
SBM	1,000	4,870,863	35 / 5 / 10	97.42
SO	2,601,997	63,497,050	65 / 9 / 18	0.12

falls within an acceptable range (-6.5% to 7.75%). Moreover, for sparse datasets, random neighbor sampling mitigates the impact of super neighbors, thereby reducing overfitting and enhancing model performance, exemplified by an improvement of 7.75% and 6.92% on the BitcoinAlpha dataset, respectively. Furthermore, as dataset size increases, the disparity in results between full-batch training and mini-batch training diminishes, demonstrating changes of 1.76% and 0.85% on the Stackoverflow dataset. Significantly, through mini-batch training, the model’s scalability is no longer constrained by the total number of nodes, thus alleviating the need for extensive GPU memory, resulting in a reduction of over 50% on the UCI dataset, leading to the establishment of a scalable model. Additionally, it was observed that in small-scale but dense datasets like Reddit-Title and Reddit-Body, nearly all nodes are sampled, causing only a marginal decrease in GPU memory usage, indicating that mini-batch training methods may not be optimal in such scenarios.

4.3 Exploration of SFDyG

In this subsection, we examined the effectiveness of Hawkes process based GNN based through ablation studies and demonstrated the impact of hyper-parameters on performance.

4.3.1 Ablation study. In modern graph neural network libraries such as PyG [6], the data structures for standard graphs and multi-graphs are identical. This implies that standard graph neural network algorithms, like GAT, can be utilized on multi-graphs formed through input snapshots fusion methods. Hence, the question arises: Is it necessary to develop dedicated algorithms for temporal multi-graphs?

As presented in Table 5, this study delves into the performance evaluation between the Hawkes process-based GAT model and the standard GAT model across eight datasets. The findings reveal that the Hawkes process-based GAT model significantly enhances the overall performance, surpassing the standard GAT by a considerable margin across all datasets. Particularly, on the AS733 dataset, the Mrr@100 metric exhibited a notable increase, skyrocketing from 0.1297 to 0.4653. This notable improvement underscores the efficacy and versatility of our proposed methodology.

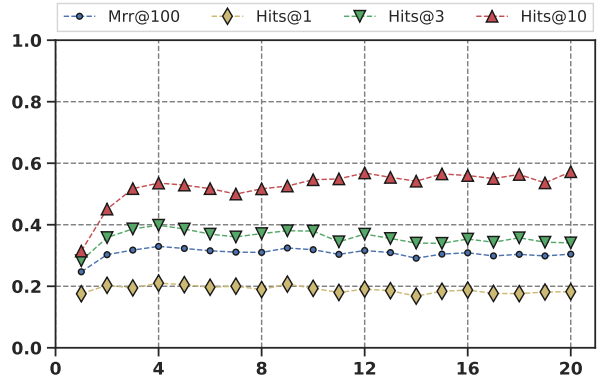


Figure 4: Performance of SFDyG-GAT on UCI dataset with various hyper-parameter settings for the input window size.

4.3.2 Hyper-parameter Sensitivity Analysis. In the SFDyG-GAT model, the window size serves as a crucial hyper-parameter. To investigate the model’s sensitivity to the window size, various window sizes were tested using the UCI dataset to analyze the performance variations, as illustrated in Figure 4. The results demonstrate

Table 4: The performance of full-batch training and mini-batch training was compared on six datasets in terms of the relative percentage change in MRR@100 (Δ MRR@100) and GPU memory usage (Δ GPU). Our experiments guarantee consistent data settings, and standardized methods for computing Mean Reciprocal Ranks (MRRs) to facilitate fair comparisons.

Dataset	SFDyG-GCN				SFDyG-GAT			
	Full-batch	Mini-batch	Δ Mrr@100	Δ GPU	Full-batch	Mini-batch	Δ Mrr@100	Δ GPU
OTC	0.3447	0.3620	\uparrow 5.02%	\downarrow 28.03%	0.3737	0.3632	\downarrow 2.81%	\downarrow 33.65%
Alpha	0.3177	0.3324	\uparrow 4.63%	\downarrow 43.23%	0.3033	0.3243	\uparrow 6.92%	\downarrow 42.87%
UCI	0.3019	0.3253	\uparrow 7.75%	\downarrow 50.03%	0.3258	0.3326	\uparrow 2.09%	\downarrow 49.18%
Title	0.4267	0.4062	\downarrow 4.80%	\downarrow 0.16%	0.5044	0.4716	\downarrow 6.50%	\downarrow 0.13%
Body	0.2795	0.2979	\uparrow 6.58%	\downarrow 0.50%	0.4046	0.4042	\downarrow 0.10%	\downarrow 0.48%
SO	0.4425	0.4347	\downarrow 1.76%	\downarrow 36.02%	0.4613	0.4652	\uparrow 0.85%	\downarrow 30.35%

Table 5: The overall performance comparison (MRR@100) on eight datasets between the standard GAT (GAT) and the Hawkes process-based GAT (SFDyG-GAT), with the relative percentage of improvements. Each experiment is executed with three random seeds, and the average performance, accompanied by the standard error, is reported.

DataSet	GAT	SFDyG-GAT	Imporve
OTC	27.80 ± 0.58	37.37 ± 0.10	34.42%
Alpha	26.64 ± 0.34	30.33 ± 1.05	13.85%
UCI	15.25 ± 1.00	32.58 ± 1.02	113.64%
Title	18.13 ± 0.34	50.44 ± 0.16	178.21%
Body	14.86 ± 1.01	40.46 ± 0.53	172.27%
AS733	12.97 ± 1.05	46.53 ± 0.49	258.75%
SBM	8.67 ± 6.88	24.02 ± 4.55	177.05%
SO	25.60 ± 1.29	46.13 ± 0.05	80.20%

that a window size of 4 represents a critical point in the model’s performance, indicating the presence of long-distance temporal dependencies within the data. Insufficient input snapshots lead to the omission of essential information. Furthermore, depicted in the figure, beyond a certain window size, the impact of the quantity of input windows on future predictions notably diminishes. This observation aligns with the Hawkes process assumption used in this study, suggesting that the influence of past events on future predictions gradually wanes over time. Taken together, these findings underscore the robustness of our proposed methodology.

5 RELATED WORKS

5.1 Dynamic Graph Neural networks

Dynamic graph representation learning aims to learn the temporal low-dimensional representations of nodes as the graph evolves over time, mainly categorized into continuous time dynamic graph (CTDG) and discrete time dynamic graph (DTDG) methods based on the form of dynamic graphs. CTDG methods treat dynamic graphs as event streams with timestamps, generating dynamic node embeddings by iteratively processing information gathered from temporal neighbors [17, 29]. Despite the success of continuous time methods [4, 27, 32], in practical applications, many datasets lack precise

timestamp information due to historical reasons, making continuous time methods inapplicable. DTDG represents the dynamic graph through a sequence of snapshots. It leverages multiple previous snapshots to predict the subsequent snapshot. The intuitive idea is to combine GNN with a time encoder such as RNN [3, 11] or Transformer [30], which, however, has high time complexity and space complexity. Recent studies have highlighted that the incorporation of extra time encoders can lead to overfitting [38]. Alternatively, single snapshot as input has been found promising by employing latent random variables [8], hyperbolic space [34] or meta-learning [35]. What sets our research apart from existing methodologies is that we fuse the multiple input snapshots, thereby obviating the necessity for additional time encoders and enabling modeling of long-term dependencies.

5.2 Scalable Graph Neural networks

It is challenging to scale GNNs to large graphs with a vast number of nodes, such as those in industrial and social applications. GNNs are typically executed in a full-batch manner, demanding more GPU memory than is often available, leading to training failures. Previous research on static graphs has proposed methods such as graph sampling [1, 2, 9], graph sparsification [18, 26], and graph partitioning [2, 22] to facilitate training on large-scale datasets. However, these existing methods are not directly transferrable to the realm of link prediction in discrete dynamic graphs. This limitation arises due to gaps still existing in terms of neighbor sampling or partitioning in both temporal and spatial dimensions. Furthermore, link prediction tasks typically require obtaining all node embeddings for contrastive learning of node pairs, necessitating full-batch training.

5.3 Hawkes Process based representation learning

Hawkes processes are powerful temporal point processes in modeling sequences [10], and have been widely studied to adapt to different scenarios. HTNE [40], a temporal network embedding method, which leverages the Hawkes process and the concept of neighborhood formation sequences to model node evolution. Nonetheless, HTNE lacks the integration of graph neural network theory and is ill-suited for discrete dynamic graphs.

6 CONCLUSION AND FUTURE WORK

This study introduces a straightforward approach to integrate multiple snapshots within the input window to improve the scalability of discrete dynamic graph models. The proposed method converts a sequence of graphs into a temporal multi-graph. by formulating a graph denoising problem with a time decay smoothing assumption, we derived GNN encoders with a time decay message-passing mechanism. This approach streamlines the application of existing scalable technologies for static graphs to the training of dynamic graphs. Specifically, we present a mini-batch training approach for the link prediction task as a demonstration of the benefits of input snapshots fusion. Extensive experimentation has validated the scalability, robustness, and versatility of our framework. This research focuses solely on the link prediction task in discrete-time dynamic graphs due to data constraints. Future directions involve incorporating meta-learning methods and expanding our framework to encompass diverse dynamic graph representation learning tasks and applications, including node classification and future link prediction.

ACKNOWLEDGMENTS

This work is supported by ...

REFERENCES

- [1] Jie Chen, Tengfei Ma, and Cao Xiao. 2018. FastGCN: Fast learning with graph convolutional networks via importance sampling. In *International Conference on Learning Representations*. International Conference on Learning Representations, ICLR.
- [2] Wei-Lin Chiang, Xuanqing Liu, Si Si, Yang Li, Samy Bengio, and Cho-Jui Hsieh. 2019. Cluster-gcn: An efficient algorithm for training deep and large graph convolutional networks. In *Proceedings of the 25th ACM SIGKDD international conference on knowledge discovery & data mining*. 257–266.
- [3] Junyoung Chung, Caglar Gulcehre, Kyunghyun Cho, and Yoshua Bengio. 2014. Empirical evaluation of gated recurrent neural networks on sequence modeling. In *NIPS 2014 Workshop on Deep Learning, December 2014*.
- [4] da Xu, chuanwei ruan, evren korpeoglu, sushant kumar, and kannan achan. 2020. Inductive representation learning on temporal graphs. In *International Conference on Learning Representations (ICLR)*.
- [5] Wenqi Fan, Yao Ma, Qing Li, Yuan He, Eric Zhao, Jiliang Tang, and Dawei Yin. 2019. Graph Neural Networks for Social Recommendation. In *The World Wide Web Conference*. <https://doi.org/10.1145/3308558.3313488>
- [6] Matthias Fey and Jan E. Lenssen. 2019. Fast Graph Representation Learning with PyTorch Geometric. In *ICLR Workshop on Representation Learning on Graphs and Manifolds*.
- [7] Justin Gilmer, Samuel S Schoenholz, Patrick F Riley, Oriol Vinyals, and George E Dahl. 2017. Neural message passing for quantum chemistry. In *International conference on machine learning*. PMLR, 1263–1272.
- [8] Ehsan Hajiramezani, Arman Hasanzadeh, Krishna Narayanan, Nick Duffield, Mingyuan Zhou, and Xiaoning Qian. 2019. Variational graph recurrent neural networks. *Advances in neural information processing systems* 32 (2019).
- [9] Will Hamilton, Zhitao Ying, and Jure Leskovec. 2017. Inductive representation learning on large graphs. *Advances in neural information processing systems* 30 (2017).
- [10] Alan G Hawkes. 1971. Spectra of some self-exciting and mutually exciting point processes. *Biometrika* 58, 1 (1971), 83–90.
- [11] Sepp Hochreiter and Jürgen Schmidhuber. 1997. Long short-term memory. *Neural computation* 9, 8 (1997), 1735–1780.
- [12] Weihua Hu, Matthias Fey, Marinka Zitnik, Yuxiao Dong, Hongyu Ren, Bowen Liu, Michele Catasta, and Jure Leskovec. 2020. Open graph benchmark: Datasets for machine learning on graphs. *Advances in neural information processing systems* 33 (2020), 22118–22133.
- [13] Sergey Ioffe and Christian Szegedy. 2015. Batch normalization: Accelerating deep network training by reducing internal covariate shift. In *International conference on machine learning*. pmlr, 448–456.
- [14] Seyed Mehran Kazemi, Rishabh Goel, Kshitij Jain, Ivan Kobyzev, Akshay Sethi, Peter Forsyth, and Pascal Poupart. 2020. Representation learning for dynamic graphs: A survey. *The Journal of Machine Learning Research* 21, 1 (2020), 2648–2720.
- [15] Diederik P Kingma and Jimmy Ba. 2014. Adam: A method for stochastic optimization. *arXiv preprint arXiv:1412.6980* (2014).
- [16] Thomas N. Kipf and Max Welling. 2017. Semi-Supervised Classification with Graph Convolutional Networks. In *International Conference on Learning Representations (ICLR)*.
- [17] Srijan Kumar, Xikun Zhang, and Jure Leskovec. 2019. Predicting dynamic embedding trajectory in temporal interaction networks. In *Proceedings of the 25th ACM SIGKDD international conference on knowledge discovery & data mining*. 1269–1278.
- [18] Jiayu Li, Tianyun Zhang, Hao Tian, Shengmin Jin, Makan Fardad, and Reza Zafarani. 2020. Sgcn: A graph sparsifier based on graph convolutional networks. In *Advances in Knowledge Discovery and Data Mining: 24th Pacific-Asia Conference, PAKDD 2020, Singapore, May 11–14, 2020, Proceedings, Part I* 24. Springer, 275–287.
- [19] Mengzhang Li and Zhanxing Zhu. 2021. Spatial-temporal fusion graph neural networks for traffic flow forecasting. In *Proceedings of the AAAI conference on artificial intelligence*, Vol. 35. 4189–4196.
- [20] Ilya Loshchilov and Frank Hutter. 2016. Sgdr: Stochastic gradient descent with warm restarts. *arXiv preprint arXiv:1608.03983* (2016).
- [21] Yao Ma, Xiaorui Liu, Tong Zhao, Yozhen Liu, Jiliang Tang, and Neil Shah. 2021. A unified view on graph neural networks as graph signal denoising. In *Proceedings of the 30th ACM International Conference on Information & Knowledge Management*. 1202–1211.
- [22] Vasimuddin Md, Sanchit Misra, Guixiang Ma, Ramanarayanan Mohanty, Evangelos Georganas, Alexander Heinecke, Dhiraj Kalamkar, Nesreen K Ahmed, and Sasikanth Avancha. 2021. Distgnn: Scalable distributed training for large-scale graph neural networks. In *Proceedings of the International Conference for High Performance Computing, Networking, Storage and Analysis*. 1–14.
- [23] Aldo Pareja, Giacomo Domeniconi, Jie Chen, Tengfei Ma, Toyotaro Suzumura, Hiroki Kamezashi, Tim Kaler, Tao B. Schardl, and Charles E. Leiserson. 2020. EvolveGCN: Evolving Graph Convolutional Networks for Dynamic Graphs. In *Proceedings of the Thirty-Fourth AAAI Conference on Artificial Intelligence*.
- [24] Patrick Reiser, Marlen Neubert, André Eberhard, Luca Torresi, Chen Zhou, Chen Shao, Houssam Metni, Clint van Hoesel, Henrik Schopmans, Timo Sommer, et al. 2022. Graph neural networks for materials science and chemistry. *Communications Materials* 3, 1 (2022), 93.
- [25] Herbert Robbins and Sutton Monro. 1951. A stochastic approximation method. *The annals of mathematical statistics* (1951), 400–407.
- [26] Yu Rong, Wenbing Huang, Tingyang Xu, and Junzhou Huang. 2019. DropEdge: Towards Deep Graph Convolutional Networks on Node Classification. In *International Conference on Learning Representations*.
- [27] Emanuele Rossi, Ben Chamberlain, Fabrizio Frasca, Davide Eynard, Federico Monti, and Michael Bronstein. 2020. Temporal Graph Networks for Deep Learning on Dynamic Graphs. In *ICML 2020 Workshop on Graph Representation Learning*.
- [28] Aravind Sankar, Yanhong Wu, Liang Gou, Wei Zhang, and Hao Yang. 2020. Dystap: Deep neural representation learning on dynamic graphs via self-attention networks. In *Proceedings of the 13th international conference on web search and data mining*. 519–527.
- [29] Rakshit Trivedi, Mehrdad Farajtabar, Prasenjeet Biswal, and Hongyuan Zha. 2019. Dyrep: Learning representations over dynamic graphs. In *International conference on learning representations*.
- [30] Ashish Vaswani, Noam Shazeer, Niki Parmar, Jakob Uszkoreit, Llion Jones, Aidan N Gomez, Łukasz Kaiser, and Illia Polosukhin. 2017. Attention is all you need. *Advances in neural information processing systems* 30 (2017).
- [31] Petar Veličković, Guillem Cucurull, Arantxa Casanova, Adriana Romero, Pietro Liò, and Yoshua Bengio. 2017. Graph Attention Networks. *6th International Conference on Learning Representations* (2017).
- [32] Xuhong Wang, Ding Lyu, Mengjian Li, Yang Xia, Qi Yang, Xinwen Wang, Xinguang Wang, Ping Cui, Yuyu Yang, Bowen Sun, et al. 2021. Apan: Asynchronous propagation attention network for real-time temporal graph embedding. In *Proceedings of the 2021 international conference on management of data*. 2628–2638.
- [33] Yongji Wu, Defu Lian, Yiheng Xu, Le Wu, and Enhong Chen. 2020. Graph Convolutional Networks with Markov Random Field Reasoning for Social Spammer Detection. *Proceedings of the AAAI Conference on Artificial Intelligence* (Jun 2020), 1054–1061. <https://doi.org/10.1609/aaai.v34i01.15455>
- [34] Menglin Yang, Min Zhou, Marcus Kalander, Zengfeng Huang, and Irwin King. 2021. Discrete-time temporal network embedding via implicit hierarchical learning in hyperbolic space. In *Proceedings of the 27th ACM SIGKDD Conference on Knowledge Discovery & Data Mining*. 1975–1985.
- [35] Jiaxuan You, Tianyu Du, and Jure Leskovec. 2022. ROLAND: Graph Learning Framework for Dynamic Graphs. In *Proceedings of the 28th ACM SIGKDD Conference on Knowledge Discovery and Data Mining* (Washington DC, USA) (KDD '22). Association for Computing Machinery, New York, NY, USA, 2358–2366. <https://doi.org/10.1145/3534678.3539300>
- [36] Bing Yu, Haoteng Yin, and Zhanxing Zhu. 2018. Spatio-temporal graph convolutional networks: a deep learning framework for traffic forecasting. In *Proceedings of the 27th International Joint Conference on Artificial Intelligence*. 3634–3640.

- [37] Kaire Zhang, Qi Cao, Gaolin Fang, Bingbing Xu, Hongjian Zou, Huawei Shen, and Xueqi Cheng. 2023. DyTed: Disentangled Representation Learning for Discrete-time Dynamic Graph. In *Proceedings of the 29th ACM SIGKDD Conference on Knowledge Discovery and Data Mining*. 3309–3320.
- [38] Yifan Zhu, Fangpeng Cong, Dan Zhang, Wenwen Gong, Qika Lin, Wenzheng Feng, Yuxiao Dong, and Jie Tang. 2023. WinGNN: Dynamic Graph Neural Networks with Random Gradient Aggregation Window. In *Proceedings of the 29th ACM SIGKDD Conference on Knowledge Discovery and Data Mining* (, Long Beach, CA, USA.) (KDD '23). Association for Computing Machinery, New York, NY, USA, 3650–3662. <https://doi.org/10.1145/3580305.3599551>
- [39] Yuan Zuo, Guannan Liu, Hao Lin, Jia Guo, Xiaoqian Hu, and Junjie Wu. 2018. Embedding Temporal Network via Neighborhood Formation. In *Proceedings of the 24th ACM SIGKDD International Conference on Knowledge Discovery & Data Mining* (London, United Kingdom) (KDD '18). Association for Computing Machinery, New York, NY, USA, 2857–2866. <https://doi.org/10.1145/3219819.3220054>
- [40] Yuan Zuo, Guannan Liu, Hao Lin, Jia Guo, Xiaoqian Hu, and Junjie Wu. 2018. Embedding temporal network via neighborhood formation. In *Proceedings of the 24th ACM SIGKDD international conference on knowledge discovery & data mining*. 2857–2866.

A RESEARCH METHODS

A.1 Details of Equation 11

In this subsection, we provide detailed descriptions of Equation 11, proving $\text{tr}(\mathbf{F}^T \mathbf{L} \mathbf{F}) = \sum_{(i,j) \in \mathcal{E}} C_{ij} \|\mathbf{F}_i - \mathbf{F}_j\|_2^2$, while $\mathbf{L} = \tilde{\mathbf{D}} - \tilde{\mathbf{A}}$. For the sake of convenience in symbolic representation, let us assume that $\mathbf{F} \in \mathbb{R}^{n \times 1}$ with elements denoted as f_1, f_2, \dots, f_n , and the process of proving in the high-dimensional case follows the same steps. By using the rule of matrix trace calculation, the left term can be changed into

$$\begin{aligned} \text{tr}(\mathbf{F}^T \mathbf{L} \mathbf{F}) &= \text{tr}(\mathbf{F} \mathbf{F}^T \mathbf{L}) \\ &= \text{tr}(\mathbf{F} \mathbf{F}^T \tilde{\mathbf{D}}) - \text{tr}(\mathbf{F} \mathbf{F}^T \tilde{\mathbf{A}}). \end{aligned}$$

Where the elements of $\mathbf{F} \mathbf{F}^T$ is

$$\begin{bmatrix} f_1 f_1 & f_1 f_2 & \cdots & f_1 f_n \\ f_2 f_1 & f_2 f_2 & \cdots & f_2 f_n \\ \vdots & \vdots & \ddots & \vdots \\ f_n f_1 & f_n f_2 & \cdots & f_n f_n \end{bmatrix}.$$

Since $\tilde{\mathbf{D}}$ is a diagonal matrix

$$\begin{bmatrix} \sum_j \mathbf{A}_{1j} C_{1j} & & \\ & \ddots & \\ & & \sum_j \mathbf{A}_{nj} C_{nj} \end{bmatrix}.$$

Therefore we have

$$\text{tr}(\mathbf{F} \mathbf{F}^T \tilde{\mathbf{D}}) = \sum_i \sum_j \mathbf{A}_{ij} C_{ij} f_i^2.$$

Since $\tilde{\mathbf{A}} = \mathbf{C} \cdot \mathbf{A}$, and trace operation only sums elements in diagonal, we have

$$\text{tr}(\mathbf{F} \mathbf{F}^T \tilde{\mathbf{A}}) = \sum_i \sum_j \mathbf{A}_{ij} C_{ij} f_i f_j.$$

Based on the above results, equation $\text{tr}(\mathbf{F} \mathbf{F}^T \tilde{\mathbf{D}}) - \text{tr}(\mathbf{F} \mathbf{F}^T \tilde{\mathbf{A}})$ can be transformed into

$$\begin{aligned} &= \sum_i \sum_j \mathbf{A}_{ij} C_{ij} f_i^2 - \sum_i \sum_j \mathbf{A}_{ij} C_{ij} f_i f_j \\ &= \frac{1}{2} \left(\sum_i \sum_j \mathbf{A}_{ij} C_{ij} f_i^2 - 2 \sum_i \sum_j \mathbf{A}_{ij} C_{ij} f_i f_j + \sum_i \sum_j \mathbf{A}_{ij} C_{ij} f_j^2 \right) \\ &= \frac{1}{2} \sum_i \sum_j \mathbf{A}_{ij} C_{ij} (f_i - f_j)^2 \\ &= \sum_{(i,j) \in \mathcal{E}} C_{ij} \|\mathbf{F}_i - \mathbf{F}_j\|_2^2, \end{aligned}$$

which completes the proof.

A.2 Proof for mini-batch algorithm

In this subsection, we provide the proofs for the correctness of the proposed mini-batch training algorithm.

LEMMA A.1. *When the parameters and inputs of a function remain unchanged, we can guarantee consistent (intermediate) results upon multiple executions.*

PROOF. When a function is deterministic, proof is unnecessary; for functions involving randomness, consistent results can be ensured for each run by specifying a random seed. \square

As a consequence, we have

COROLLARY A.1.1. *Using $\mathcal{H}^{\text{full}}$ to represent the intermediate result of full-batch training, \mathcal{H}^{s1} for the forward result of step 1 in mini-batch training, and \mathcal{H}^{s3} for the forward result of step 3 in mini-batch training, we establish the equivalence $\mathcal{H}^{\text{full}} = \mathcal{H}^{\text{s1}} = \mathcal{H}^{\text{s3}}$.*

COROLLARY A.1.2. *The final loss of full-batch training, denoted as $\mathcal{L}^{\text{full}}$, is equivalent to that in step 2 of mini-batch training, denoted as \mathcal{L}^{s2} : $\mathcal{L}^{\text{full}} = \mathcal{L}^{\text{s2}}$, as we assume the negative edges are identical.*

COROLLARY A.1.3. *As the backward propagation only execute once in each iteration, to streamline the representation, we employ $\tilde{\cdot}$ to denote mini-batch training. Then we have these partial derivatives of Equation 15 are the equivalent: $\frac{\partial \mathcal{L}}{\partial H} = \tilde{\frac{\partial \mathcal{L}}{\partial H}}$, $\frac{\partial \mathcal{L}}{\partial F} = \tilde{\frac{\partial \mathcal{L}}{\partial F}}$, $\frac{\partial \mathcal{L}}{\partial G} = \tilde{\frac{\partial \mathcal{L}}{\partial G}}$. Where Z represents the vector of all z_{ij} .*

THEOREM A.2 (EQUIVALENCE THEOREM). *The proposed three-step mini-batch training method is equivalent to the full-batch training method when the result of negative sampling are the same.*

PROOF. First we show $\frac{\partial \mathcal{L}}{\partial Z} = \tilde{\frac{\partial \mathcal{L}}{\partial Z}}$. For every element z_{ij} in Z , using the chain rule we have

$$\begin{aligned} \frac{\partial \mathcal{L}}{\partial z_{ij}} &= \frac{\partial \mathcal{L}}{\partial \hat{y}_{ij}} \frac{\partial \hat{y}_{ij}}{\partial z_{ij}} \\ &= \left(\frac{y_{ij}}{\hat{y}_{ij}} + \frac{1 - y_{ij}}{1 - \hat{y}_{ij}} \right) (\hat{y}_{ij}(1 - \hat{y}_{ij})) \\ &= y_{ij}(1 - \hat{y}_{ij}) + (1 - y_{ij})\hat{y}_{ij} \\ &= \begin{cases} \hat{y}_{ij}, & \text{if } y_{ij} = 0, \\ 1 - \hat{y}_{ij}, & \text{if } y_{ij} = 1, \end{cases} \end{aligned}$$

which implies $\frac{\partial \mathcal{L}}{\partial Z}$ only depends on all \hat{y}_{ij} which is equivalent as shown in Corollary A.1.2. More importantly, it is in the linear form

of \hat{y}_{ij} , therefore the partial derivatives across mini-batches can be accumulated by summation. Then we have

$$\frac{\partial \mathcal{L}}{\partial \mathcal{F}} = \frac{\partial \widetilde{\mathcal{L}}}{\mathcal{F}}, \frac{\partial \mathcal{L}}{\partial \mathcal{H}} = \frac{\partial \widetilde{\mathcal{L}}}{\mathcal{F}}, \frac{\partial \mathcal{L}}{\partial \mathcal{G}} = \frac{\partial \widetilde{\mathcal{L}}}{\mathcal{G}},$$

using the chain rule and result from Corollary A.1.3, which completes the proof. \square

A.3 Complexity Analysis

In this subsection, we provide the detailed descriptions for time and space analysis in Table 1.

Time complexity. According to the results presented ClusterGCN [2], the time complexity of message-passing based GNN is given by $O(L|E|F + LNF^2)$. The DySAT involves obtaining node embeddings for T snapshots within a given time window, which requires a time complexity of $O(TL|E|F + TLNF^2)$. Following this, the self-attention is utilized to encode temporal information for N nodes in T snapshots. The time complexity of the self-attention mechanism is $O(NT^2F)$, while the feature transformation complexity is $O(NTF^2)$. Consequently, the time complexity of DySAT can be expressed as $O(TL|E|F + TLNF^2 + NT^2F)$. Considering usually $LF > T$, then it can be written as $O(TL|E|F + TLNF^2)$. In the case of EvolveGCN, RNN is used to update the parameters at each GNN step in the time window, and RNN performs feature transformation for all nodes in each snapshot, resulting in a time complexity of $O(NTF^2)$. Thus, the total time complexity of EvolveGCN is $O(TL|E|F + TLNF^2)$. In the Roland algorithm, the time window T is set to 1 and no time encoder is utilized, leading to a complexity of $O(L|E|F + LNF^2)$ for a single window. SFDyG merges T snapshots in the time window into a single multi-graph, with the number of edges being $T|E|$. Therefore, for the full-batch training of SFDyG, denoted as SFDyG-F, the time complexity is $O(TL|E|F + LNF^2)$. For the mini-batch training version of SFDyG denoted as SFDyG-B, each node requires feature aggregation from $O(d^L)$ neighbors, resulting in a time complexity of $O(Nd^L F^2)$.

Memory complexity. Similarly, Based on the conclusions from the ClusterGCN [2], the message passing based GNN has a space complexity of $O(L|E|F + LF^2)$. Consequently, the space complexity of the GNN component in DySAT is $O(TL|N|F + TLF^2)$. The self-attention mechanism requires storing the attention matrix with $O(T^2)$, outputs ($O(TF)$), and feature transformation parameters $O(F^2)$. Therefore, the space complexity of the self-attention component becomes $O(|N|T^2 + |N|TF + F^2)$. Typically, with $LF > T$, leading to an overall space complexity of $O(TL|N|F + TLF^2)$ for DySAT. The RNN part of EvolveGCN needs to store all intermediate results as parameters for GNN, resulting in a space complexity of $O(T|N|FL + F^2)$. Consequently, the combined space complexity becomes $O(TL|N|F + TLF^2)$. As Roland has a window size of 1, its space complexity is the same as that of a single GNN, which is $O(L|E|F + LF^2)$. In the case of the full-batch SFDyG-F, the input edge number is $T|E|$, resulting in a space complexity of $O(LT|E|F + LF^2)$. For the mini-batch trained SFDyG-F, a mini-batch can have bd^L edges, resulting in a space complexity of $O(bd^L F + LF^2)$.

B EXPERIMENT DETAILS

B.1 Description of Datasets

In our experiments, we utilize a combination of synthetic and publicly available benchmark

Stochastic Block Model.¹ (SBM for short) SBM is a widely employed random graph model utilized for simulating community structures and evolutions. The data utilized in this study was obtained from the GitHub repository of EvolveGCN [23].

Bitcoin OTC.² (OTC for short) OTC is a who-trusts-whom network among bitcoin users who engage in trading activities on the platform <http://www.bitcoin-otc.com>. The data set may be used for predicting the polarity of each rating and forecasting whether a user will rate another one in the next time step.

Bitcoin Alpha.³ (Alpha for short) Alpha is created in the same manner as is BC-OTC, except that the users and ratings come from a different trading platform, <http://www.btc-alpha.com>.

UC Irvine messages.⁴ (UCI for short) UCI is an online community of students from the University of California, Irvine, wherein the links of this social network indicate sent messages between users. Link prediction is a standard task for this data set.

Autonomous systems.⁵ (AS for short) Autonomous Systems (AS) constitute a communication network of routers that exchange traffic flows with their peers. This dataset can be utilized for predicting future message exchanges.

Reddit-Title and Reddit-Body.⁶ The network of hyperlinks between subreddits is derived from hyperlinks found in posts. These hyperlinks can appear in either post titles or bodies, resulting in two distinct datasets.

Stack Overflow.⁷ (SO for short) The dataset presents interactions within the Stack Overflow platform. Nodes in the dataset represent users, while directed edges indicate the flow of answer activity between users.

B.2 Description of Baselines

Several baseline models exist for predicting links in discrete dynamic graphs. There are discrepancies in the choice of datasets, data preprocessing techniques, model implementation approaches, and metric computation criteria among these models. To ensure a fair comparison, we consulted relevant open-source code, authored all baseline methods, and rectified certain evident inaccuracies in the code. Consequently, our results may exhibit variations from those presented in the original publication.

DySAT [28] computes node representations through joint self-attention along the two dimensions of the structural neighborhood and temporal dynamics.

EvolveGCN [23]: adapts the GCN to compute node representations, and captures the dynamism of the graph sequence by using an RNN to evolve the GCN parameters.

¹<https://github.com/IBM/EvolveGCN>

²<http://snap.stanford.edu/data/soc-sign-bitcoin-otc.html>

³<http://snap.stanford.edu/data/soc-sign-bitcoin-alpha.html>

⁴<http://konect.uni-koblenz.de/networks/opsahl-ucsocial>

⁵<http://snap.stanford.edu/data/as-733.html>

⁶<https://snap.stanford.edu/data/soc-RedditHyperlinks.html>

⁷<https://snap.stanford.edu/data/sx-stackoverflow.html>

VGRNN [8]: a hierarchical variational model that introduces additional latent random variables to jointly model the hidden states of a graph recurrent neural network (GRNN).

WinGNN [38]: is a GNN model that employs a meta-learning strategy and introduces a novel random gradient aggregation mechanism. Notice that there was a serious error in its open-source code, which misunderstood the relationship between input snapshots and predicted target snapshots. As a result, awaiting-prediction edges were inadvertently introduced into the model’s input, causing grossly exaggerated outcomes. This issue has been rectified in our code.

ROLAND [35]: views the node representations at different GNN layers as hierarchical node states and recurrently updates them. We present results of the moving average variant of Roland, which can be trained in our GPU environment for the StackOverflow dataset.

HTGN [34] maps the dynamic graph into hyperbolic space, and incorporates hyperbolic graph neural network and hyperbolic gated recurrent neural network to obtain representations.

B.3 Evaluation Metrics

The MRR score is the average of the reciprocal ranks of the positive samples within the negative samples, formally,

$$MRR = \frac{1}{N} \sum_{i=1}^N \frac{1}{rank(p_i)}.$$

Sample as it is, several statistical approaches have been utilized in previous research to calculate this metric. The potential options include determining whether to convert the target directed snapshot to an undirected graph, whether to average MRR values of multiple snapshots directly (macro) or weight them by the number of positive edges (micro), and whether negative sampling in the test set should be generated consistently or randomly for each iteration.

The purpose of this study is to minimize the influence of random effects on the metrics, ensure reproducibility of experimental results, and enable the model to generate meaningful predictions of practical significance. To accomplish this, we employ directed micro-MRR and predetermined test set negative sampling.

B.4 Experiment Setup

B.4.1 Running Environment. . We perform our comparisons on a Ubuntu 20.04.4 LTS server with Intel Xeon 32-Core Processor, 200 GB RAM, and an NVIDIA V100S-32GB Tensor Core GPU. SFDyG is implemented with Python 3.11.4 with PyTorch 2.1.2 and torch_geometric 2.4.0 framework.

B.4.2 Hyper-parameter Settings. . In all experiments, unless otherwise specified, we ensured consistency by utilizing a standardized set of hyperparameters. This approach encompassed utilizing dummy node features (a vector of all ones) to avoid over-fitting, generating 10 negative samples per training data edge, and 100 negative samples per testing data edge. Negative sampling for testing was executed only once to maintain experiment reproducibility. The training window size was set to 10, comprising 9 input snapshots and one target snapshot. The default dropout rate was 0.1, the learning rate was 0.001, the hidden layer size was 64 and the patience of early stopping was 10 epochs. Additionally, the Adam [15] was

used as the optimizer for gradient descent and Cosine Annealing learning rate scheduler [20] was used to accelerate training.

B.5 Additional Results

Additional performance metrics of the model, including Hit@1, Hit@3, and Hit@10, are elaborated in Table 6, Table 7, and Table 8 separately within the appendix.

Received 20 February 2007; revised 12 March 2009; accepted 5 June 2009

Table 6: Overall performance (Hit@1) comparison on eight datasets (%) is omitted). Our experiments guarantee consistent data settings, and standardized methods for computing Mean Reciprocal Ranks (MRRs) to facilitate fair comparisons. Each experiment is conducted using three random seeds, and the average performance is reported along with the standard error.

Methods	OTC	Alpha	UCI	Title	Body	AS733	SBM	SO
DySAT	0.18 ± 0.25	1.03 ± 1.31	0.27 ± 0.21	0.82 ± 0.44	0.20 ± 0.21	17.72 ± 0.50	0.77 ± 0.61	OOM.
Evolve-o	2.61 ± 0.18	2.54 ± 0.54	2.87 ± 0.00	OOM.	13.69 ± 0.01	35.70 ± 0.00	16.14 ± 0.00	OOM.
Evolve-h	2.28 ± 0.08	2.67 ± 0.29	1.95 ± 1.31	26.64 ± 0.07	13.69 ± 0.01	35.70 ± 0.00	16.14 ± 0.00	OOM.
VGRNN	1.99 ± 0.20	2.28 ± 0.49	2.92 ± 0.10	OOM.	OOM.	33.54 ± 1.18	14.25 ± 0.63	OOM.
Roland	14.10 ± 0.47	14.81 ± 1.16	8.17 ± 2.30	33.73 ± 0.25	26.71 ± 0.41	27.36 ± 5.44	0.03 ± 0.04	24.04 ± 0.31
WinGNN	0.58 ± 0.29	0.34 ± 0.09	0.10 ± 0.10	2.04 ± 0.65	1.03 ± 0.87	3.85 ± 0.82	1.04 ± 0.26	OOM.
HTGN	1.49 ± 0.50	1.44 ± 0.39	3.84 ± 2.87	19.21 ± 1.55	9.55 ± 6.08	7.38 ± 3.29	OOM.	OOM.
SFDyG-GCN	22.58 ± 0.43	18.75 ± 0.60	17.14 ± 0.47	29.18 ± 0.56	14.54 ± 0.54	29.63 ± 0.37	18.55 ± 0.19	32.56 ± 0.12
SFDyG-GAT	28.78 ± 0.09	22.63 ± 1.07	20.91 ± 1.19	37.55 ± 0.27	27.74 ± 0.65	35.25 ± 0.43	18.37 ± 5.97	33.53 ± 0.07

Table 7: Overall performance (Hit@3) comparison on eight datasets (%) is omitted). Our experiments guarantee consistent data settings, and standardized methods for computing Mean Reciprocal Ranks (MRRs) to facilitate fair comparisons. Each experiment is conducted using three random seeds, and the average performance is reported along with the standard error.

Methods	OTC	Alpha	UCI	Title	Body	AS733	SBM	SO
DySAT	0.62 ± 0.88	1.71 ± 1.75	1.71 ± 1.38	0.86 ± 0.46	0.22 ± 0.24	18.73 ± 0.92	2.08 ± 1.43	OOM.
Evolve-o	4.30 ± 0.18	3.16 ± 0.54	4.10 ± 0.00	OOM.	16.68 ± 0.04	45.56 ± 0.00	21.32 ± 0.00	OOM.
Evolve-h	3.71 ± 0.08	3.36 ± 0.35	3.35 ± 0.99	30.33 ± 0.02	16.70 ± 0.04	45.56 ± 0.00	21.32 ± 0.00	OOM.
VGRNN	3.86 ± 0.47	4.86 ± 0.21	4.61 ± 0.13	OOM.	OOM.	44.86 ± 0.83	19.68 ± 0.48	OOM.
Roland	33.71 ± 0.29	35.16 ± 1.44	22.25 ± 3.09	52.04 ± 0.51	42.80 ± 0.60	41.16 ± 5.93	0.38 ± 0.54	40.86 ± 0.14
WinGNN	1.91 ± 0.50	1.22 ± 0.57	0.86 ± 0.93	4.34 ± 0.83	1.81 ± 1.52	5.18 ± 1.79	1.34 ± 0.12	OOM.
HTGN	3.48 ± 1.50	3.95 ± 0.88	5.81 ± 3.36	25.51 ± 2.07	14.55 ± 8.25	10.85 ± 5.85	OOM.	OOM.
SFDyG-GCN	42.16 ± 0.12	39.26 ± 0.75	34.85 ± 0.09	48.01 ± 0.78	30.06 ± 0.99	53.33 ± 0.12	22.57 ± 0.23	47.99 ± 0.13
SFDyG-GAT	41.11 ± 0.36	32.57 ± 1.45	38.19 ± 0.78	57.19 ± 0.07	46.02 ± 0.52	49.32 ± 0.58	23.39 ± 4.48	52.02 ± 0.20

Table 8: Overall performance (Hit@10) comparison on eight datasets (%) is omitted). Our experiments guarantee consistent data settings, and standardized methods for computing Mean Reciprocal Ranks (MRRs) to facilitate fair comparisons. Each experiment is conducted using three random seeds, and the average performance is reported along with the standard error.

Methods	OTC	Alpha	UCI	Title	Body	AS733	SBM	SO
DySAT	1.81 ± 1.70	3.16 ± 3.45	5.57 ± 4.61	1.05 ± 0.49	2.05 ± 2.81	19.55 ± 0.86	6.43 ± 5.20	OOM.
Evolve-o	17.44 ± 0.29	13.51 ± 0.19	14.63 ± 0.10	OOM.	24.97 ± 0.05	49.99 ± 0.00	29.16 ± 0.00	OOM.
Evolve-h	15.90 ± 0.21	14.20 ± 0.89	12.00 ± 3.92	35.03 ± 0.02	25.01 ± 0.04	49.99 ± 0.00	29.16 ± 0.00	OOM.
VGRNN	14.17 ± 0.90	12.76 ± 0.19	11.62 ± 0.31	OOM.	OOM.	56.89 ± 1.06	27.94 ± 0.31	OOM.
Roland	57.46 ± 1.41	59.30 ± 0.86	45.20 ± 3.08	74.07 ± 0.61	67.05 ± 0.52	66.79 ± 5.55	4.36 ± 6.17	65.25 ± 0.17
WinGNN	6.72 ± 2.73	6.91 ± 4.36	4.18 ± 3.92	11.47 ± 1.11	2.96 ± 2.10	8.28 ± 4.06	1.93 ± 0.04	OOM.
HTGN	12.05 ± 2.82	9.95 ± 0.92	13.16 ± 2.35	33.97 ± 2.47	23.60 ± 10.05	17.48 ± 7.31	OOM.	OOM.
SFDyG-GCN	52.75 ± 0.20	52.70 ± 0.60	58.04 ± 0.75	71.22 ± 0.75	60.75 ± 0.36	79.32 ± 0.45	32.64 ± 0.38	71.63 ± 0.09
SFDyG-GAT	48.89 ± 0.12	42.29 ± 0.39	53.04 ± 1.91	75.85 ± 0.05	66.34 ± 0.19	70.31 ± 0.74	32.78 ± 1.54	73.15 ± 0.03